FABRICATION, TREATMENT, AND TESTING
OF MATERIALS AND STRUCTURES

Features of ZnS-Powder Doping with a Mn Impurity during Synthesis and Subsequent Annealing

N. E. Korsunska^, Yu. Yu. Bacherikov, T. R. Stara, V. P. Kladko, N. P. Baran, Yu. O. Polishchuk, A. V. Kuchuk, A. G. Zhuk, and Ye. F. Venger

Lashkaryov Institute of Semiconductor Physics, National Academy of Sciences of Ukraine, Kyiv, 03028 Ukraine

^ e-mail: kors@isp.kiev.ua

Abstract—Luminescence, electron spin resonance, and X-ray diffraction (XRD) methods were used to investigate the features of ZnS-powder doped by Mn impurity during self-propagating high-temperature synthesis and subsequent annealing. The obtained powder consists of ZnS microcrystals with mainly hexagonal phase $(80 \pm 5)\%$. It was found, that after synthesis Mn presents not only in the form of non-uniformly distributed microscopic impurities in ZnS, but also in the form of Mn metal nanocrystals. Thermal annealing at 800°C leads to the additional doping of ZnS from metallic Mn, to the redistribution of the embedded Mn in the volume of microcrystals, and to the ZnS oxidation. At the same time, the ratio between the cubic and hexagonal phases does not change. It was shown that annealing causes a decrease in the concentration of the defects responsible for the luminescence-excitation bands, which correspond to transitions from the ground to the excited states of the Mn^{2+} ion. As a result of annealing, there is also a change in XRD coherent domain size. Simultaneously, the intensity of peaks in the luminescence-excitation spectrum with wavelengths of 375 and 395 nm was changed. The causes of these changes and the nature of the corresponding bands are discussed.

DOI: 10.1134/S1063782613050138

1. INTRODUCTION

Zinc sulfide doped with various impurities is an important material for optoelectronic devices emitting in a wide spectral range. In particular, doping of ZnS with copper is used for generating blue–green luminescence [1, 2], and doping with Mn, for generating orange emission [3]. In this case, the impurity can be introduced either by diffusion from the surface into a previously synthesized material or directly during synthesis.

It is obvious that an important factor determining the luminescence properties of phosphors is the impurity distribution in material. This problem is reasonably well investigated and described in available publications for ZnS films and single crystals [4, 5]. At the same time, these issues are much less investigated for the powder material, although, the latter is widely used for fabricating luminophors. In particular, such information for the powdered ZnS, produced by high-temperature self propagated synthesis (SHS) is almost absent. At the same time, this method has a number of advantages in comparison with other methods of ZnS fabrication from the point of view of power consumption, ecological safety, and cost of the installation. In addition, it makes it possible to obtain both single crystals and a powder material including nanoscale ZnS and to dope them directly during growth.

It should be noted, that the SHS is a procedure with exothermic reaction and high temperature (2500–3000°C) during ZnS synthesis is its feature. This results in the crystallization of compounds formed during synthesis, which makes it possible to use X-ray diffraction analysis to investigate the phase composition of the obtained material.

In this study, the results of investigating the photoluminescence (PL) spectra, the luminescence-excitation spectra (LES), electron spin resonance (ESR), and X-ray diffraction (XRD) of ZnS-powder samples obtained by the SHS method and doped with manganese during synthesis are presented. In addition, the effect of thermal annealing on these characteristics is also studied.

2. EXPERIMENTAL

The investigated ZnS:Mn semiconductor was synthesized by the SHS method at temperatures providing the interaction of sulfur and zinc [6–8] and doped during growth via a MnCl-containing mixture. The relation (in mass fractions) between the initial materials was as follows: 63% Zn, 34% S, and 1% MnCl. Subsequent thermal annealing at 800°C was performed for 240 min in a laboratory quartz furnace. The atmosphere access to the annealed powder was restricted by a granulated-coal gas gate. As it was shown previously [9], the time t_h of sample heating to

PL intensity, arb. units
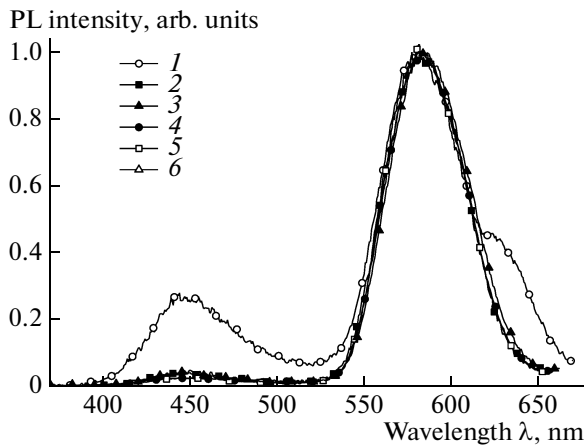
Fig. 1. Spectra of photoluminescence (PL) for the (*1*) initial and (*2–6*) annealed ZnS:Mn samples. Time of furnace heating to the annealing temperature, min: (*2*) 15, (*3*) 30, (*4*) 60, (*5*) 120, and (*6*) 240.

the annealing temperature can affect the sample characteristics. Therefore, the time t_h of annealing was varied from 15 to 240 min.

The PL spectra and LES were detected at room temperature using an SDL-2 installation. The LES were measured under excitation by the light of a DKSSh-150 xenon lamp through an MDR-12 monochromator, and the PL spectra were measured under excitation by the light of N_2 laser with the wavelength $\lambda_{ex} = 337$ nm. The X-ray diffraction investigations were carried out using a Philips X'Pert-MRD X-ray diffractometer (CuK_α; the wavelength $\lambda = 0.15418$ nm) in the Bragg–Brentano geometry. The XRD coherent domain size D_{hkl} (*hkl* are the Miller indices of the reflecting planes) was determined from the Scherrer formula $D_{hkl} = 0.9\lambda/\beta_{hkl}\cos\theta$, where λ is the emission wavelength, β_{hkl} is the reflection angular width at half maximum, and θ is the peak angular position. To determine β_{hkl} more precisely, the peaks were approximated by the Pseudo-Voigt function. The ESR spectra were measured at room temperature using a Varian E-12 installation. The modulation frequency was 100 kHz, and the modulation amplitude was 0.1–0.2 mT.

3. EXPERIMENTAL RESULTS

3.1 Photoluminescence

In Fig. 1, the PL spectra of the initial and annealed ZnS:Mn samples are shown. As can be seen from Fig. 1, the PL spectrum of the ZnS:Mn powder before annealing consists of three bands with peaks at the wavelengths $\lambda_{max} = 455$, 584, and 630 nm. Since the intensity of the band with $\lambda_{max} = 584$ nm varied much more weakly after annealing than the intensity of the other bands (within 30%, which is within the limits of

the alignment error), the spectra in Fig. 1 are normalized to this band.

The broad band with $\lambda_{max} \approx 584$ nm dominant in the spectrum is typical of Mn-doped ZnS. According to published data [10–14], it consists of a set of individual bands with $\lambda_{max} = 557$, 578, and 600 nm caused by different localization of the Mn impurity atoms in the ZnS crystal lattice. The band with $\lambda_{max} = 600$ nm is associated with Mn^{2+} ions at octahedral interstitial sites, and the band with $\lambda_{max} = 578$ nm is related to Mn^{2+} ions near dislocations or point defects [10, 11]. As regards the nature of the band with $\lambda_{max} = 557$ nm, the majority of authors [10–14] consider that it is caused by centers formed by manganese ions located in the areas of the zinc sublattice of severe lattice damage In some studies [15, 16], it is assumed that the emission band with $\lambda_{max} = 557$ nm is also complex and caused by the emission from several centers located in the tetrahedral crystal-lattice sites of zinc sulfide surrounded with defects.

A PL band with $\lambda_{max} = 630$ nm is usually observed in heavily doped samples, and the authors of [17] relate it to transitions in the Mn^{2+} ion in the α-MnS phase.

The band with the shortest wavelength $\lambda_{max} \approx 455$ nm present in the PL spectrum of ZnS:Mn is likely complex. According to the published data, in this PL-spectral region of ZnS, the following bands are observed: the SA band with $\lambda_{max} \approx 505$ nm [18], a band with $\lambda_{max} = 496$ nm related to the associate center ($V_{Zn}Cl_S$) [19, 20], bands with $\lambda_{max} = 405$ and 466 nm related to V_S and Zn_i, respectively, and also bands with $\lambda_{max} \approx 404$ and 435 nm induced by the presence of oxygen in ZnS [3, 21].

After annealing, the intensity of the bands with $\lambda_{max} = 455$ and 630 nm substantially decreases; the band with $\lambda_{max} = 630$ nm is not being revealed in the spectrum. It should be noted that these changes are almost independent of the time of furnace heating to the annealing temperature.

In Fig. 2a, we show the LES corresponding to the maximum of the band of 578 nm for the unannealed and annealed samples without recalculation of these spectra for the apparatus function of the installation. Since the short-wavelength wings of the spectra to the position of the interband excitation edge hardly vary during annealing, LES was normalized to the interband excitation edge. As it can be seen from Fig. 2a, it is possible to single out the following bands in the LES of the unannealed sample: $\lambda_{ex} = 364$, 396, 417, 467, and 492 nm.

According to [2, 22], the bands at ~364 and ~396 nm can be related to transitions in the oxygen cluster with the participation of the Cu impurity. In particular, the authors of [2, 23] suppose that these are transitions from the Cu_{Zn} acceptor level to the conduction band and from the Cu_{Zn} level to the Cu_i level,

respectively. It should be noted, that the position of these bands depends on the oxygen content [23], and their presence can be caused by an uncontrollable copper impurity accompanying MnCl in our case. Other features of the LES are related to the absorption bands in the Mn^{2+} ion that corresponds to well-known transitions from the ground state of the ion $^6A_1$ to the excited states $^4T_1$, $^4T_2$, $^4E_1$, and $^4A_1$ [11, 24]. Apparently, the band at 396 nm also contains one of the "manganese" bands ($^6A_1 \longrightarrow {}^4T_1$) with $\lambda_{ex} = 391$ nm.

It is worth noting that the emission of a Mn ion is sensibilized; i.e., the exciting-light energy is absorbed by certain centers (sensitizers), the role of which in ZnS:Mn can be played by closely located defects including Mn_{Zn}, Cl, O, etc. Then, this energy is transferred to the emitting manganese ion (activator) [18]. In this case, if the defect absorption band is overlapped with the absorption bands of Mn emitting ions, and also upon their excitation via Mn_{Zn}, manganese bands manifest themselves in LES.

After annealing, the intensity of the manganese bands decreases, and these changes depend only weakly on the time of furnace heating to the annealing temperature (Fig. 2b, curves *4*, *5*). At the same time, the LES in the region of 350−400 nm depends on t_h. In particular, a band at $\lambda_{ex} = 375$ nm appears during annealing. In Fig. 2b, the dependences of the PL intensity upon excitation by light with the wavelengths $\lambda_{ex} = 362$, 375, and 395 nm on t_h (curves *1−3*) were shown. As it can be seen, the PL intensity at first increases for such excitation and, then, decreases at $t_h = 240$ min. However, these changes are insignificant for $\lambda_{ex} = 362$ nm and are caused, apparently, by the contribution of bands with $\lambda_{ex} = 375$ and 395 nm, the intensity of which varies much more severely.
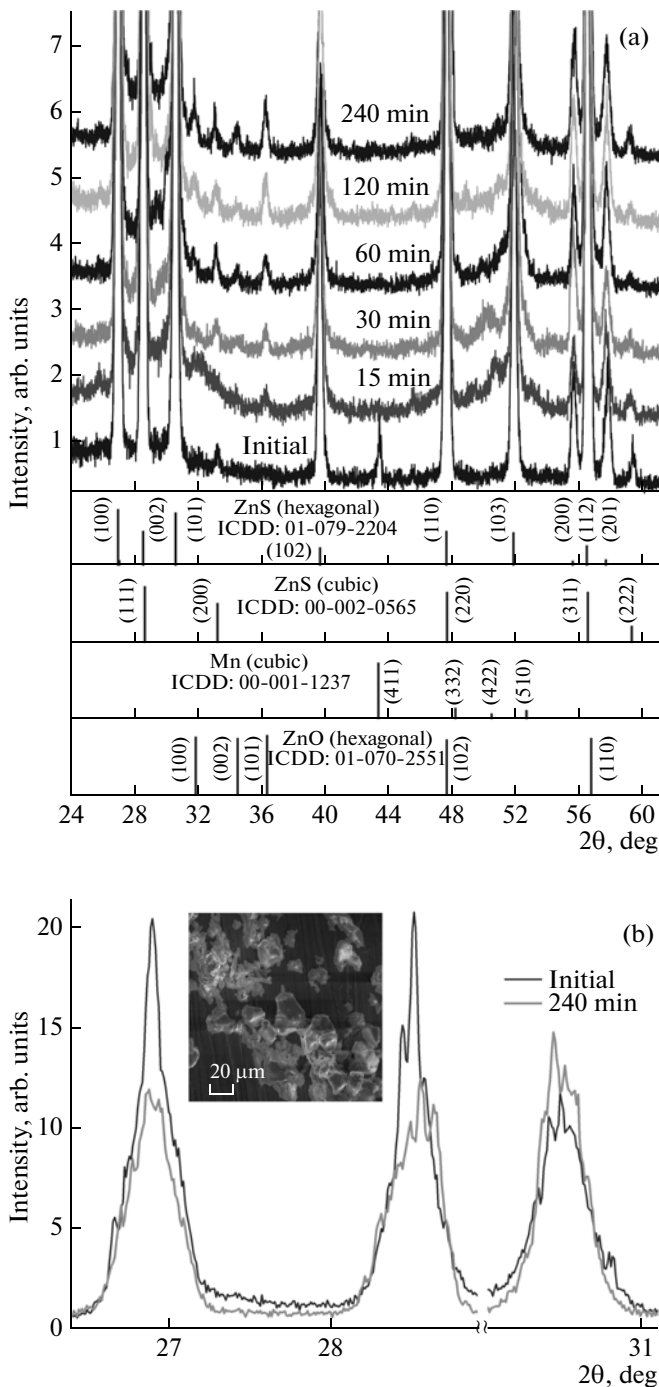
3.2 X-Ray Diffraction

The results of phase composition investigation of ZnS:Mn powder by the method of X-ray diffraction are shown in Fig. 3. As it can be seen from Fig. 3a, the initial powder consists mainly of the nonequilibrium hexagonal (wurtzite) and equilibrium cubic (zinc blend) phases of ZnS. Strong reflections from the hexagonal phase indicate its dominant role, which is a characteristic of ZnS powders with a high concentration of Mn. The contribution of the hexagonal phase estimated by the method described in [25] amounts to $(80 \pm 5)\%$ and is practically invariable after annealing at $T = 800°C$. In addition, the cubic phase of metal Mn (the peak at $2\theta \approx 43.3°$) is also present in the initial powder. The average size of Mn crystallites amounts to $D \approx (40 \pm 5)$ nm. Despite the fact that annealing doesn't lead to any changes in the ratio between the ZnS hexagonal and cubic phases, it causes a number of transformations in the diffraction spectra. In particular, the reflection from the Mn crystal disappears after
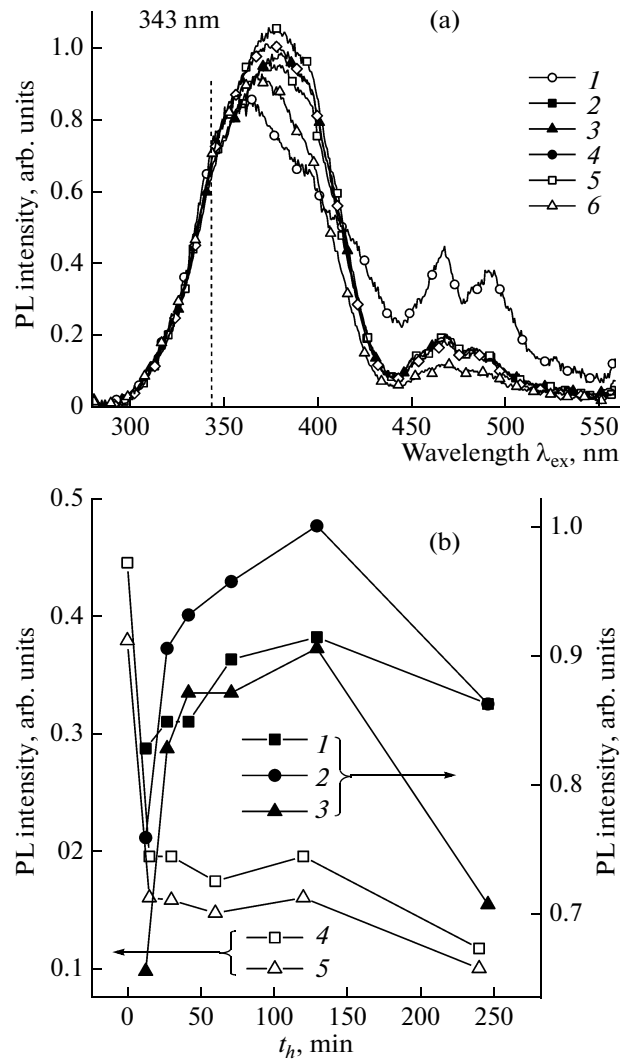
Fig. 2. (a) Spectra of excitation of photoluminescence (PL) for the (*1*) unannealed and (*2−6*) annealed ZnS:Mn samples. Time of furnace heating to the annealing temperature, min: (*2*) 15, (*3*) 30, (*4*) 60, (*5*) 120, and (*6*) 240. (b) Dependences of the intensity of photoluminescence (PL) for ZnS:Mn upon excitation stimulated by emission with $\lambda_{ex} = $ (*1*) 362, (*2*) 375, (*3*) 395, (*4*) 467, and (*5*) 491 nm on t_h. The point $t_h = 0$ corresponds to an unannealed sample.

annealing (irrespective of t_h), and reflections from the ZnO hexagonal phase appear. This suggests that annealing results in the disappearance of Mn nanocrystals and also in ZnS oxidation, which is caused by the presence of oxygen in the atmosphere where the powders were annealed.

As it can be seen from Fig. 3b, the reflections from the ZnS hexagonal phase have a fine structure (consists of a number of discrete peaks), which indicates the discrete distribution of the interplanar distances (the lattice parameter) in crystallites. This distribution is caused, apparently, by the presence of areas with a different deformation degree of the ZnS lattice, which

Fig. 3. (a) Spectra of X-ray diffraction for powder ZnS:Mn before and after annealing at 800°C for times of furnace heating to the annealing temperature within the range 15 to 240 min, and also a bar diagram for the cubic (ZnS, Mn) and hexagonal (ZnS, ZnO) phases; (b) magnified fragment of the radiograph of powder ZnS:Mn before and after annealing at 800°C for a heating time of 240 min; the inset shows a ZnS:Mn-powder image obtained by scanning electron microscopy.

is related, most likely, to a different Mn concentration in them. From Fig. 3b, it also follows that annealing for $t_h = 240$ min results in a more homogeneous distri-
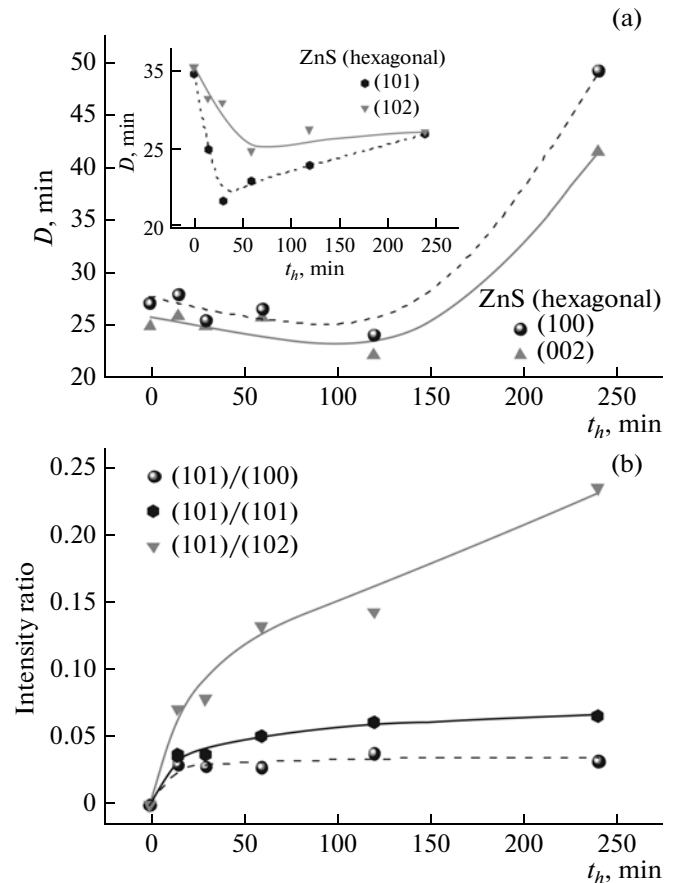
Fig. 4. Dependences of (a) the size (D) of the coherent scattering regions for the ZnS hexagonal phase and (b) the ratio of the intensity of the (101) reflection for ZnO to the intensities of the (100), (101), and (102) reflections for ZnS hexagonal phases on t_h; $t_h = 0$ corresponds to the unannealed sample.

bution of the lattice parameter of ZnS crystallites. In this case, we also observe changes in the peak intensity and width at half maximum of certain ZnS hexagonal phase reflections, which are related to the effect of annealing on the coherent domain size (D).

In Fig. 4a, we show the annealing effects on the D value of the ZnS hexagonal phase in more detail. It can be seen that irrespective of the reflection, D first decreases to a minimum and, then, increases with the time of sample heating to the annealing temperature. However, quantitative variations of D size drastically differ for different reflections. In particular, for (100) and (200) reflections, the decrease of D with increasing t_h is insignificant, while the subsequent increase is sharper. At the same time, for the (101) and (102) reflections, an inverse relationship (a sharp decrease to a minimum and a weak increase after it) is observed. Thus, a significant decrease of D in the directions $[10\bar{1}1]$ and $[10\bar{1}2]$ at small t_h and also its almost double increase in the [0001] and $[10\bar{1}0]$ directions at $t_h =$
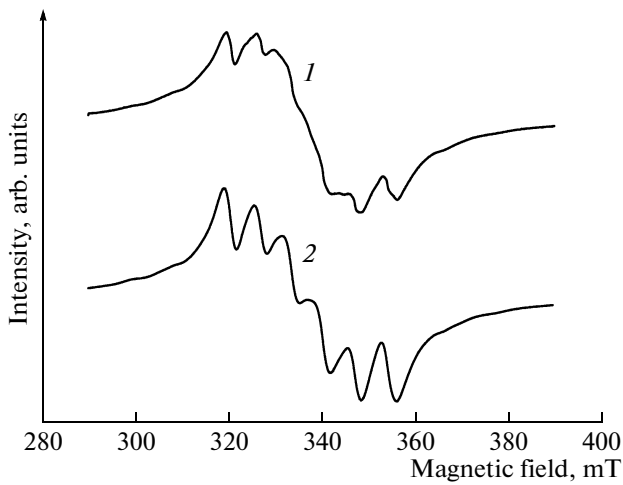
Fig. 5. ESR differential spectra of the (*1*) initial and (*2*) annealed samples; $t_h = 15$ min.

240 min indicate the anisotropic character of the variation in this parameter. It is necessary to note that the coherent domain size for the ZnS cubic phase varies insignificantly with increasing t_h and amounts to $D = (30 \pm 5)$ nm. From Fig. 4b, it follows that ZnS oxidation is most significant at small t_h and is dependent on the ZnS hexagonal phase reflections.

3.3 Electron Spin Resonance

The differential ESR spectra for the initial and annealed (for $t_h = 15$ min) samples are shown in Fig. 5. The spectrum of the initial sample (curve *1*) consists of a broad line, against the background of which six lines are detected, which is a characteristic for Mn^{2+} (Mn_{Zn}) paramagnetic centers. In addition, it contains a weakly pronounced structure, which also can be related to the Mn^{2+} centers. Because there is a small amount of the cubic phase in the samples under investigation in addition to the hexagonal phase, it is possible to assume that the observable set of lines is related to Mn_{Zn} centers in two ZnS phases. In this case, the weakly pronounced structure corresponds to the cubic phase.

After annealing (curve *2*), the intensity of the broad line decreases, and the intensity of lines from the Mn^{2+} centers increases; in this case, the weakly pronounced structure present before annealing is not observed. This fact and also the values of the superfine-interaction constant and the spectroscopic-splitting factor testify that the spectrum of ESR from the Mn^{2+} centers observed after annealing corresponds to the Mn_{Zn} centers in zinc sulfide hexagonal modification. The large width of these lines is caused by the significant Mn concentration in the grains. We note that the
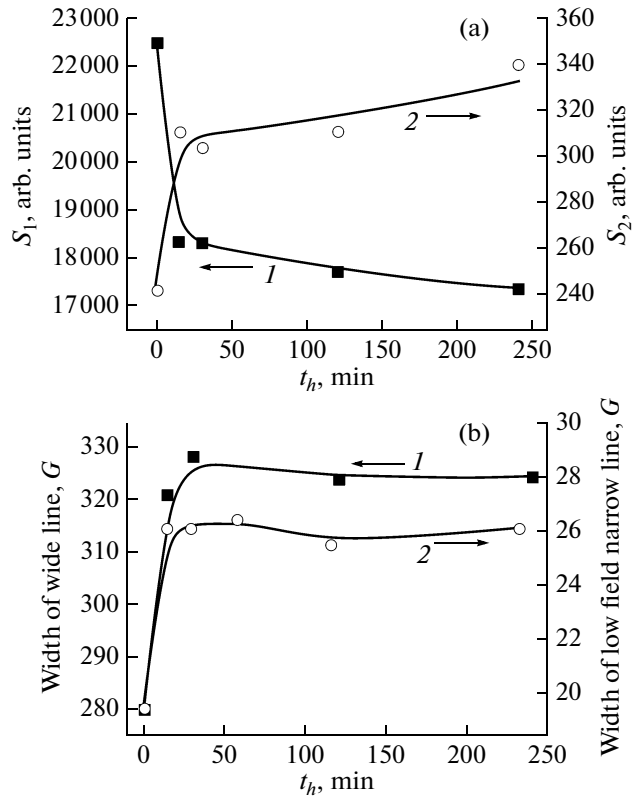

Fig. 6. Dependence of the (*a*) areas under the curves and (*b*) half widths of the (*1*) broad and (*2*) narrow lines on t_h; $t_h = 0$ corresponds to the unannealed sample.

shape of the ESR spectra in the annealed samples is independent of t_h.

Figure 6a shows the t_h dependences of the area enveloped by the broad line (S_1) and the sum of the areas under the narrow lines (S_2) obtained from the decomposition of the integrated spectra. As it can be seen from Fig. 6, S_1 and S_2 substantially vary as a result of annealing but depend on t_h much more weakly.

The variations in the intensities of the broad and narrow lines are accompanied with an increase in their width. In Fig. 6b, we present the values of the width at half maximum (further—half width) of the broad line determined from the integral-spectra decomposition, and the half width of the low-field line from the Mn^{2+} centers determined from the differential spectra before and after annealing. As it can be seen from the figure, the half width of the lines substantially changes as a result of annealing and is almost independent of t_h, which agrees with the weak dependence on t_h for the values of S_1 and S_2.

It should be noted that an ESR spectrum similar to the described one (the superposition of the broad line and six broadened lines from the Mn^{2+} centers) was observed in ZnS powder, which contained 1 mol % of Mn [26]. With increasing of Mn content, the half

width of the six narrow lines increased, and their intensity decreased. For 5 mol %, only the broad line was observed. Its half width decreased with increasing concentration of introduced Mn [26]. The increase in the half width of the narrow lines with the concentration of introduced Mn is associated with the dominant role of the magnetic dipole–dipole interaction between the centers, whereas the occurrence of the broad line with increasing concentration of Mn is caused by the increasing role of exchange interaction [26].

It is substantial that the broad-line area varies as a result of annealing much stronger, than the sum of the areas of the narrow lines. It is possible to specify two possible causes of this. First, it is possible that the main fraction of the incorporated Mn is in a different charge state with a large orbital momentum (for example, in interstitial sites) and is not detected at room temperature due to rapid spin–lattice relaxation. Second, at high concentrations, Mn can form antiferromagnetic pairs, which gives no ESR signal.

4. DISCUSSION OF RESULTS

As it can be seen from the results of the XRD investigation, when doping ZnS with manganese during SHS, the introduced impurity is not only penetrate into ZnS microcrystals, but also present in the form of Mn nanocrystals. The annealing results in the disappearance of the X-ray reflection from metallic Mn. Simultaneously, the ESR signal from the Mn_{Zn} centers in ZnS increases. Since there is a low probability of Mn evaporation at 800°C, it is possible to assume that there is an additional doping of ZnS grains from Mn nanocrystals during annealing, which is one of the causes of the increasing ESR signal. On the other hand, simultaneously with the increasing ESR signal from Mn_{Zn} centers, the intensity of the broad ESR signal related to Mn, as well as the intensity of the PL band with $\lambda_{max} = 630$ nm, which is attributed to transitions in Mn^{2+} ions in the α-MnS phase decreases.

Two ESR signals related to Mn are indicative of the presence of regions with different concentrations in the samples under investigation. In this case, the broad signal corresponds to regions with a higher concentration [26]. These regions, in principle, can be the regions of the $Zn_xMn_{1-x}S$ alloy as well as metallic-Mn or MnS-compound inclusions.

Since the XRD reflection caused by the metallic-manganese nanocrystals disappears after annealing, while the intensity of the broad ESR line decreases by only ~20%, it is possible to assume that this line is not related to metallic manganese. As regards the MnS phase, it was not observed in the XRD spectra. In addition, the measurements of the ESR spectra of powder MnS showed that the half width of the detected line (~15 mT) is much narrower than the half width of the line observed in the samples investigated (~30 mT). Therefore, it is logical to associate the broad line with Mn clusters in ZnS, where the Mn ions are located at distances larger than those in the case of MnS. These clusters are located, obviously, in more heavily doped regions representing the $Zn_xMn_{1-x}S$ alloy. This agrees with the data of [26] in which a broad line was observed for an incorporated Mn concentration more than 1%. It is obviously, that the PL band with $\lambda_{max} = 630$ nm can be related to heavily-doped ZnS regions. An additional argument against its relation to the α-MnS phase is the fact that, according to the data of [17], no luminescence band related to Mn is observed in α-MnS. Because the components are distributed nonuniformly in alloys, it is possible that the band with $\lambda_{max} = 630$ nm is related to the inclusions corresponding to the solubility limit for Mn in ZnS.

A decrease in the intensity of the broad ESR signal after annealing with a simultaneous increase in the signal intensity caused by "isolated" Mn_{Zn} centers means that the Mn impurity is nonuniformly distributed in the grain volume after synthesis, and the annealing results in its partial redistribution. This agrees with the variation in the half widths of the broad and narrow lines. In fact, an increase in the half width of the broad line is indicative of a decrease in the Mn concentration in more heavily doped regions, and an increase in the half width of the narrow lines is related to an increase in its concentration in less heavily doped regions. Apparently, a decrease in the PL-band intensity with $\lambda_{max} = 630$ nm is related to a decreasing Mn concentration in the heavily doped regions. It should be noted, that despite the fact that there is an increase in the Mn_{Zn}-center concentration upon annealing, the intensity of the band with $\lambda_{max} \approx 584$ nm varies insignificantly. It can be caused by several circumstances. One of them can be that the main fraction of the manganese incorporated into the ZnS lattice is in an undamaged lattice and, thus, participates in no luminescence. Another reason can be that ESR detects the Mn_{Zn} centers in the entire grain volume, while the PL method detects the centers only in their surface region due to the high absorption coefficient of the excitation light. Finally, concentration quenching of the PL is also possible.

Thus, after synthesis, the impurity is not incorporated into the grain completely and, also it is distributed in the grain volume nonuniformly. These features are caused, obviously, by the severe nonequilibrium nature of the synthesis process and can be partly eliminated by thermal annealing.

However, annealing also results in other changes in the defect system. In particular, the intensity of the manganese bands in the LES decreases during annealing. Since the Mn_{Zn} concentration in the ZnS grains increases (ESR) after annealing, but the intensity of the manganese bands decreases, they, obviously, are not related to the excitation transfer from the Mn_{Zn} centers to the luminescence centers and are caused by the presence of other defects. The growth in the con-

centration of Mn incorporated into the grains doesn't allow also attributing a decrease in the intensity of these bands to an increase in the distance between the luminescence centers and other defects involved in their excitation. Therefore, it is possible to assume that the decrease in intensity of the manganese bands in the LES is caused by the decreasing concentration of these defects.

Annealing results also in a decrease in the contribution of the band with $\lambda_{max} = 455$ nm to the PL spectrum. Since the Mn_{Zn} concentration increases during annealing, the decrease in the intensity of the band with $\lambda_{max} = 455$ nm could be accounted for by the embedding of Mn into a Zn vacancy, if centers of self-activated luminescence, including V_{Zn}, give a substantial contribution to this band. However, it turns out that the intensity of the band with $\lambda_{max} = 455$ nm decreases not only during thermal annealing, but also upon long-term storage of samples in air, when the concentration of the ESR Mn^{2+} (Mn_{Zn}) centers does not change. Therefore, to clarify the causes of the decrease in intensity of the band with $\lambda_{max} = 455$ nm, further investigations are necessary.

During annealing, there is also a change in the contribution of the defects causing the LES bands with $\lambda_{ex} = 375$ and 395 nm, and also a change in the D value in the hexagonal ZnS phase. It is significant that the intensity of the bands with $\lambda_{ex} = 375$ and 395 nm and also the D value nonmonotonically depend on t_h.

It should be noted that D value ~$(25-50)$ nm in the hexagonal ZnS phase is much smaller than the ZnS-grain size ~$(5-50)$ μm estimated by scanning electron microscopy. Hence, there is a significant number of intercrystalline boundaries inside the grains. The block structure of the grains is confirmed also by the fine structure of the X-ray-diffraction peaks. With t_h increasing, D, at first, decreases and then increases, which is indicative of the competition of two processes. Because t_h-dependent ZnS oxidation takes place during annealing, a decrease of D can be related to a decrease in the sizes of ZnS blocks due to the formation of ZnO. An increase in D value can be explained by an increase in the size of certain blocks and the disappearance of others, which leads to a decrease in the number of intercrystalline boundaries. We assume that exactly the anisotropic migration of these boundaries, which is likely a thermally activated process, results in a substantial increase in D value in the [0001] and [$10\bar{1}0$] directions at long t_h. It is confirmed by the modification of the fine structure of the corresponding reflections (increase in their intensity and decrease in the numbers of discrete peaks within them). It should be noted, that the similar processes of the migration and disappearance of intercrystalline boundaries were observed in nanocrystalline materials under the action of applied mechanical stresses [27]

and were explained by stress-stimulated migration and the subsequent annihilation of block boundaries.

As it can be seen from Fig. 4b, the oxidation of ZnS also has an anisotropic character, which is retained with increasing t_h. In fact, the different decrease of D in different crystallographic directions at small t_h takes place.

The competition of the processes of oxidation and increasing in block sizes can result in a nonmonotonic variation in the number of extended defects with increasing t_h. Upon oxidation, ZnO/ZnS interfaces are formed, and the number of intercrystalline boundaries decreases upon a change in the block sizes. This correlates with the nonmonotonic variation of the LES-peak intensity with $\lambda_{ex} = 375$ and 395 nm. Their intensity increases, when the process favoring an increase in the number of extended defects is dominant, and decreases with their number (D increases). It enables us to assume that these peaks are caused by defects near ZnO/ZnS interfaces or intercrystalline boundaries.

5. CONCLUSIONS

The PL, PL-excitation, and ESR spectra, X-ray diffraction, and also the effect of annealing at 800°C on these characteristics were investigated for powder ZnS:Mn obtained by the SHS method and doped during synthesis. It was shown that the initial samples represent a mixture of hexagonal and cubic phases of ZnS (with ~80% content of the hexagonal phase) and consist grains of 5−50 μm in size. The samples also contain nanocrystalline inclusions of metallic Mn. As it is shown by the presence of two types of signals in the ESR spectra caused by Mn, after synthesis, the impurity is distributed in the grains nonuniformly. A broad ESR line, characteristical for Mn_{Zn} in ZnMnS alloys, and the PL band with $\lambda_{max} = 630$ nm, correspond to regions with an increased concentration of Mn.

Annealing results in additional doping of the grains from metal Mn, impurity redistribution in the grain bulk, and ZnS oxidation. The first two processes are almost independent of the sample heating time to the annealing temperature, while the oxide fraction increases with t_h. It is shown that annealing causes a decrease in the concentration of defects responsible for the luminescence-excitation bands corresponding to transitions from the ground to the excited states of the Mn^{2+} ion. As a result of annealing, there is also a change in the coherent domain size and in the intensities of the LES peaks with $\lambda_{ex} = 375$ and 395 nm. It is shown that the D value and the intensity of the LES peaks with $\lambda_{ex} = 375$ and 395 nm nonmonotonically depend on t_h. It is assumed that the D variations is caused by the competition between the processes of oxidation and block-boundary disappearance. On the basis of the obtained dependences, it was concluded

that the LES peaks with $\lambda_{ex} = 375$ and 395 nm are caused by defects located near the extended defects.

REFERENCES

1. L. A Gromov, and V. A. Trofimov, Zh. Fiz. Khim. **55**, 2629 (1981).

2. N. K. Morozova, D. A. Mideros, V. G. Galstyan, and E. M. Gavrishchuk, Sov. Phys. Semicond. **42**, 1023 (2008).

3. A. M. Gurvich, *Introduction to the Physical Chemistry of Crystal Phosphors* (Vyssh. Shkola, Moscow, 1971) [in Russian].

4. Y. V. Vorobiev, S. J. Sandoval, J. G. Hernandez, S. V. Kozitsky, R. V. Zakharchenko, and V. N. Zakharchenko, Superficies Vacio **8**, 37 (1999).

5. M. K. Samokhvalov and R. R. Davydov, Tech. Phys. Lett. **28**, 1049 (2002).

6. I. E. Molodetskaya, S. V. Kozitskii, and D. D. Polishchuk, Izv. AN SSSR, Neorg. Mater. **27**, 1142 (1991).

7. Yu. V. Vorob'ev, V. N. Zakharchenko, and S. V. Kozitskii, Kvant. Elektron. (Kiev) **4**, 73 (1995).

8. S. V. Kozytckyy, V. P. Pysarskyy, and D. D. Polishchuk, Phys. Chem. Solid State **4**, 749 (2003).

9. Yu. Yu. Bacherikov, I. S. Golovina, N. V. Kitsyuk, M. A. Mukhlyo, V. E. Rodionov, and A. A. Stadnik, J. Func. Mater. **11**, 343 (2004).

10. N. D. Borisenko, M. F. Bulanyi, F. F. Kodzhespirov, and B. A. Polezhaev, Zh. Prikl. Spektrosk. **55**, 452 (1991).

11. M. F. Bulanyi, B. A. Polezhaev, T. A. Prokof'ev, and I. M. Chernenko, J. Appl. Spectrosc. **67**, 282 (2000).

12. N. D. Borisenko and B. A. Polezhaev, Zh. Prikl. Spektrosk. **53**, 1020 (1990).

13. N. D. Borisenko, V. I. Klimenko, and B. A. Polezhaev, Zh. Prikl. Spektrosk. **50**, 475 (1989).

14. W. Busse, H. Gumlish, R. O. Tornqvist, and V. Tanninen, Phys. Status. Solidi A **76**, 553 (1983).

15. M. F. Bulanyi, A. A. Gorban', A. V. Kovalenko, B. A. Polezhaev, and T. A. Prokof'ev, Izv. Vyssh. Uchebn. Zaved., Fiz. **12**, 66 (2002).

16. W. Busse, H.-E. Gumlich, A. Geoffroy, and R. Parrot, Phys. Status Solidi B **93**, 591 (1979).

17. N. Karar, F. Singh, and B. R. Mehta, J. Appl. Phys. **95**, 656 (2004).

18. N. P. Golubeva and M. V. Fok, Zh. Prikl. Spektrosk. **17**, 261 (1972).

19. V. F. Tunitskaya, T. F. Filina, E. I. Panasyuk, and Z. P. Ilyukhina, Zh. Prikl. Spektrosk. **14**, 239 (1971).

20. *Physics and Chemistry of II–VI Compounds*, Ed. by M. Aven and J. S. Prener (North-Holland, Amsterdam, 1967; Mir, Moscow, 1970).

21. T. V. Butkhuzi, A. N. Georgobiani, E. Zada-Uly, B. T. El'tazarov, and T. G. Khulordava, Trudy Fiz. Inst. AN **182**, 140 (1987).

22. N. K. Morozova, D. A. Mideros, and N. D. Danilevich, Semiconductors **43**, 162 (2009).

23. N. K. Morozova, D. A. Mideros, E. M. Gavrishchuk, and V. G. Galstyan, Fiz. Tekh. Poluprovodn. 42, 131 (2008) [Sov. Phys. Semicond. **42**, 131 (2008).

24. V. F. Agekyan, Phys. Solid State **44**, 2013 (2002).

25. Y. T. Nien, I. G. Chen, C. S. Hwang, and S. Y. Chu, J. Electroceram. **17**, 299 (2006).

26. T. H. Yeom, Y. H. Lee, T. S. Hahn, and M. H. Oh, J. Appl. Phys. **79**, 1004 (1996).

27. M. Yu. Gutkin and N. K. Dynkin, Phys. Solid State **54**, 798 (2012).

Translated by V. Bukhanov